Pergamon

PII: S0301-9322(96)00077-8

Int. J. Multiphase Flow Vol. 23, No. 4, pp. 613–629, 1997
© 1997 Elsevier Science Ltd. All rights reserved
Printed in Great Britain
0301-9322/97 $17.00 + 0.00

SLOW VISCOUS FLOWS OF HIGHLY CONCENTRATED SUSPENSIONS—PART II: PARTICLE MIGRATION, VELOCITY AND CONCENTRATION PROFILES IN RECTANGULAR DUCTS

A. SHAULY, A. AVERBAKH, A. NIR and R. SEMIAT
Department of Chemical Engineering, Technion Institute of Technology, Haifa 32000, Israel

(Received 2 February 1996; in revised form 2 October 1996)

Abstract—The utilization of the laser-Doppler velocimetry technique in concentrated suspensions facilitated a direct measurement of particle migration velocities. Velocity measurements of dispersions at moderate and high particle concentrations, in the range of $0.3 < \phi_s < 0.50$, showed a direct connection between particle lateral migration and changes in suspension velocity profiles. The longitudinal profiles lose their Newtonian shape at high concentrations.

A qualitative agreement is shown in this work between the measured lateral and longitudinal velocity profiles and model calculations based on a phenomenological model. © 1997 Elsevier Science Ltd.

Key Words: concentrated suspensions, laser–Doppler velocimetry, particles migration, viscous flow

1. INTRODUCTION

In a preceding communication, henceforth termed as Part I, Averbakh *et al.* (1997) have described an experimental method of measuring velocities in slow viscous flows of highly concentrated suspensions. The method is based on laser–Doppler anemometry. The penetration of the laser light into the bulk of the concentrated suspension is facilitated by matching the refractive indices of the dispersed and continuous phases.

Measurement of velocities in the bulk of concentrated suspensions has particular importance since there is an accumulated experimental evidence that the flow of such mixtures is inherently different from that of an equivalent homogeneous liquid. Karnis *et al.* (1966) reported that when a suspension flows in a tube the velocity profile has a blunt shape. The reports of Gadala-Maria and Acrivos (1980) and Leighton (1985) of a gradual decrease in the viscosity of concentrated suspension when measured in a Couette viscometer were later attributed by Leighton and Acrivos (1987a,b) to a non homogeneous particle distribution in the sheared suspension which is caused by shear-induced particle migration. The latter also appears to be the mechanism which is responsible to the phenomenon of particles resuspension from a sediment layer subjected to shear by a slow viscous flow (Leighton and Acrivos 1986; Schaflinger *et al.* 1990). It is now well accepted that in a sheared concentrated suspension, particles migrated due to multiparticles interactions. In a homogeneous suspension with constant shear the particle migrate as in a self diffusion process. However, when local changes exist particles will migrate along three gradients, the gradient of particle concentration, the gradient of shear rate and the gradient of effective suspension viscosity. These mechanisms, described by Leighton and Acrivos (1987a) can also be expressed in terms of changes in the particles interaction frequency and changes of the local effective viscosity. Phillips *et al.* (1992) presented a phenomenological expression for the particle migration flux which is based on the above ideas and which can be used in material and momentum balances to obtain particle concentration and velocity distribution in flowing suspensions.

The mechanisms suggested for the particle migration (Leighton and Acrivos 1987a) indicated that it is not possible to characterize the phenomenon using a single particle shear-induced diffusion coefficient. In fact particles can diffuse *against* concentration gradients as in the case in all experiments reporting particle migration which start with a uniform homogeneous suspension.

Recently, Seifu *et al.* (1994) have shown that when the model suggested by Phillips *et al.* (1992) is applied to various flowing suspensions it predicts a considerable reduction in the effective energy dissipation in the flows which follow the particles redistribution. Seifu *et al.* (1994) also indicated that the model formulated by Phillips *et al.* (1992) can be recast as a flux of a single entity with a single (variable) diffusion coefficient.

It would be of great interest to directly detect particle migration in a flowing suspension. Eckstein *et al.* (1977) and Leighton and Acrivos (1987b) reported measurements of a single shear induced diffusion coefficient. Phillips *et al.* (1992), using NMR techniques measured particles concentrations in a Couette device and have demonstrated the redistribution of the profiles following particles migrations. In Part I we have described in detail an experimental method to detect local velocities in a flowing suspension. This method is based on laser–Doppler anemometry and was used to measure velocities in a flow of concentrated suspensions in a rectangular duct. A similar experimental geometry and optical technique was recently reported by Koh *et al.* (1994). They have measured velocity profiles and particle concentration for flows in a rectangular cavity. The results were limited to particle volume fraction of 0.3 or less since the suspension tended to lose its transparency and the increased turbidity prevented operation with higher concentrations. Although migration effects at these concentration are limited, Koh *et al.* (1994) reported changes in measured local particle concentration along the center line of the cavity as well as reshaping the velocity profiles. These results are significant since the model of Phillips *et al.* (1992) does not predict changes after such a short duration of flow. The attempt to compare the result to one dimensional steady concentration profiles is not very meaningful since the experimental flow conditions are far from that situation.

Direct measurements of local drift velocities in transient states is the main subject of this work. The approach which we have taken in Part I and in this communication is to measure the longitudinal velocity profiles and to detect lateral velocities in a rectangular duct. Since the particle concentration distribution is far from steady, transient migration velocities are expected to exist. These will depend on the shear intensity manifested by the total flow rate and the initial uniform particle concentration.

In section 2 we formulate governing equations for the suspension flow and the particle migration in the rectangular duct, based on the phenomenological flux model of Phillips *et al.* (1992). The flux is recast in the form of a particle migration potential. Calculated results for final and transient states are presented. The bulk of the measured results and their interpretation are brought in section 3 where velocity distributions and migration fluxes are reported and discussed.

2. THEORETICAL PREDICTIONS

2.1. Formulation

The shear-induced migration of particles is driven by concentration gradients and by bulk shear gradients (Leighton and Acrivos 1987a). A phenomenological model based on these principles (Phillips *et al.* 1992) yields the particle flux

$$\mathbf{J} = -K_C a^2 \phi \nabla(\phi\dot{\gamma}) - K_\mu a^2 \frac{\dot{\gamma}\phi^2}{\mu} \nabla\mu \qquad [1]$$

where $\dot{\gamma}$ is the magnitude of the bulk velocity gradient, μ is the suspension effective viscosity and a is the radius of the particle. K_C and K_μ are dimensionless coefficients of O(1). Note that particles can migrate against concentration gradients, as was also evident in experiments (Gadala-Maria and Acrivos 1980), if the part of the flux involving $\nabla\dot{\gamma}$ is large enough. Note also that no flux is predicted if $\phi\dot{\gamma}\mu^\lambda$ is constant with $\lambda = K_\mu/K_C$. In view of the form of [1] we, therefore, introduce a 'particle migration potential' (see also Seifu *et al.* 1994)

$$P = \ln(\phi\dot{\gamma}\mu^\lambda) \qquad [2]$$

with which the particle shear-induced flux [1] becomes

$$\mathbf{J} = -D\nabla P \qquad [3]$$

where $D = K_C a^2 \gamma \phi^2$.

The dynamic change of particle concentration, ϕ, along the flow is governed by the particle balance

$$\frac{D\phi}{Dt} = \nabla\cdot(D\nabla P) \qquad [4]$$

and should be evaluated simultaneously with the momentum equation. We assume that, due to the high effective viscosity resulting from the high particle concentration and at low volumetric flow rate, inertia effects are neglected. Thus the local flow is fully developed and the local stress and velocity fields obey the incompressible viscous flow equations for Newtonian fluids

$$\nabla\cdot\boldsymbol{\sigma} = \mathbf{0}$$

$$\nabla\cdot\mathbf{u} = \mathbf{0} \qquad [5]$$

where $\boldsymbol{\sigma} = \mu\,(\nabla\mathbf{u} + \nabla\mathbf{u}^t) - pI$ with p being the pressure. Note that the distance required to obtain a fully developed velocity profile is expected to be much smaller than the duct width (Schlichting 1965). To a first approximation we further assume that the bulk flow is unidirectional along the rectangular duct (z-direction), the pressure is uniform in a cross-section and the pressure variations along the flow can be obtained step by step in a quasi-linear manner. The simultaneous particle balance and suspension momentum equations become

$$w\frac{\partial\phi}{\partial z} = \nabla\cdot(K_C a^2\gamma\phi^2\nabla P) \qquad [6]$$

and

$$\mu\nabla^2 w + \nabla\mu\cdot\nabla w = \frac{\partial p}{\partial z} \qquad [7]$$

with ∇ having non zero components only in the cross section plane and w being the velocity component in the z direction. At the entrance to the rectangular duct the suspension is well mixed and homogeneous. The effective viscosity is uniform in the cross section and [7] is reduced to the Newtonian form.

The solution of the above equations requires the use of a model for the effective viscosity of a concentrated suspension. Following Phillips *et al.* (1992) we have adopted the Newtonian relative viscosity model of Krieger (1972)

$$\mu = \mu_0\left(1 - \frac{\phi}{\phi_m}\right)^{-m} \qquad [8]$$

where μ_0 is the viscosity of the suspending fluid, ϕ_m is the maximum possible particle volume fraction, taken as $\phi_m = 0.6$, and $m = 1.82$ is an empirical constant.

Once [6] is solved the local particle flux, $\mathbf{J}$, at each cross section can be obtained from [1] or [3] and the particle migration velocity components (u, v in x and y directions, respectively) can be evaluated directly, at each point, from

$$\mathbf{u} = \frac{\mathbf{J}}{\phi}. \qquad [9]$$

It is convenient to render the problem non-dimensional by normalizing the various variables using the typical dimensions of table 1.

Equations [6] and [7] then reduce to the form

$$w\frac{\partial\phi}{\partial z} = \nabla\cdot(\gamma\phi^2\nabla P) \quad \text{and} \quad \mu\nabla^2 w + \nabla\mu\cdot\nabla w = \frac{\partial p}{\partial z}, \qquad [10]$$

where the variables and gradients are now nondimensional.

Table 1. Normalization

Variable	Normalizing typical dimension
x,y	b—half duct width
w	w_{max}—maximum initial velocity at center
ϕ	ϕ_m—maximum particle concentration
z	$b^3/K_C a^2 \phi_m$
μ	μ_0
$\frac{dp}{dz}$	$w_{max}\mu_0/b^2$
γ	w_{max}/b
u,v	$K_C a^2 \phi_m w_{max}/b^2$
e^P	$\phi_m w_{max}\mu_0^*/b$

Equations [10] are subject to appropriate conditions at the solid boundaries, i.e. no slip condition for the momentum equation and no particle penetration at the wall, and to initial uniform particle concentration with the associated Newtonian velocity distribution. They were solved numerically using standard finite difference approach. At every step the momentum balance was solved using the SOR method. Next the velocity gradient magnitude, γ, was calculated. The local concentration profile was then obtained by solving the first equation in [10] using a semi-implicit ADI algorithm (Press *et al.* 1992). In each such step the pressure gradient was corrected by keeping the total flow rate and the total particle flux constant. The first is required by the incompressibility condition and the latter is obtained by integrating equation [6] in a cross section

$$\int w\frac{\partial \phi}{\partial z}dA = \int \nabla\cdot\mathbf{J}dA = 0. \qquad [11]$$

Final profiles of velocity and particle concentration can be obtained by caring the transient solution to long distances along the duct. These can also be evaluated directly by assuming a uniform value for P in the flow cross section and solving for the resulting velocity and concentration profiles. The latter procedure was iterated until convergence.

2.2. *Calculated results*

Final state flow. Figure 1 shows the profiles of the velocity w and the magnitude of velocity gradient γ in a quarter of the duct cross section at the entrance region where the concentration distribution and the effective viscosity are uniform and the flow is assumed Newtonian. Clearly, the shear rate gradients are relatively low along the x-axis near the center of the duct and also at the four corners of the duct. It is thus expected that, due to the shear-induced diffusion model, particles migrate toward these low shear regimes from the high shear regimes and accumulate there. This effect is visible in figure 2 where we plotted the profiles of particle concentration and effective viscosity at the final steady state far down stream for a suspension with an average concentration $\phi_s = 0.4$. It is evident that ϕ near the center along the x axis and at the corners increased considerably beyond the initial value, $\phi_s = 0.4$. Simultaneously, of course, the concentration is depleted at the relatively high shear zones, i.e., along the duct walls. The resulting effective viscosity in the duct cross-section is highly non-uniform. It increases considerably at the stagnant corners and at the duct center it becomes singular since the concentration there is maintained by the flow and the particle migration process at $\phi = \phi_m$. These changes in the concentration and the effective viscosity are further reflected in the final steady state velocity and shear rate profiles as depicted in figure 3. It is interesting to note that the general shapes remain similar to those of the initial state. However, one can notice that a wide region of low γ has developed along the x axis flattening the velocity profiles there. This effect is seen vividly in the cross sectional final velocity profiles shown in figure 4 for several average suspension concentrations relative to the initial Newtonian one. It is evident that the profile along the short cross-section axis (figure 4(b)) becomes flat in its middle for all high concentrations. The profile along the long cross-section axis remains almost unchanged though becomes somewhat rounder to satisfy overall continuity (figure 4(a)). The

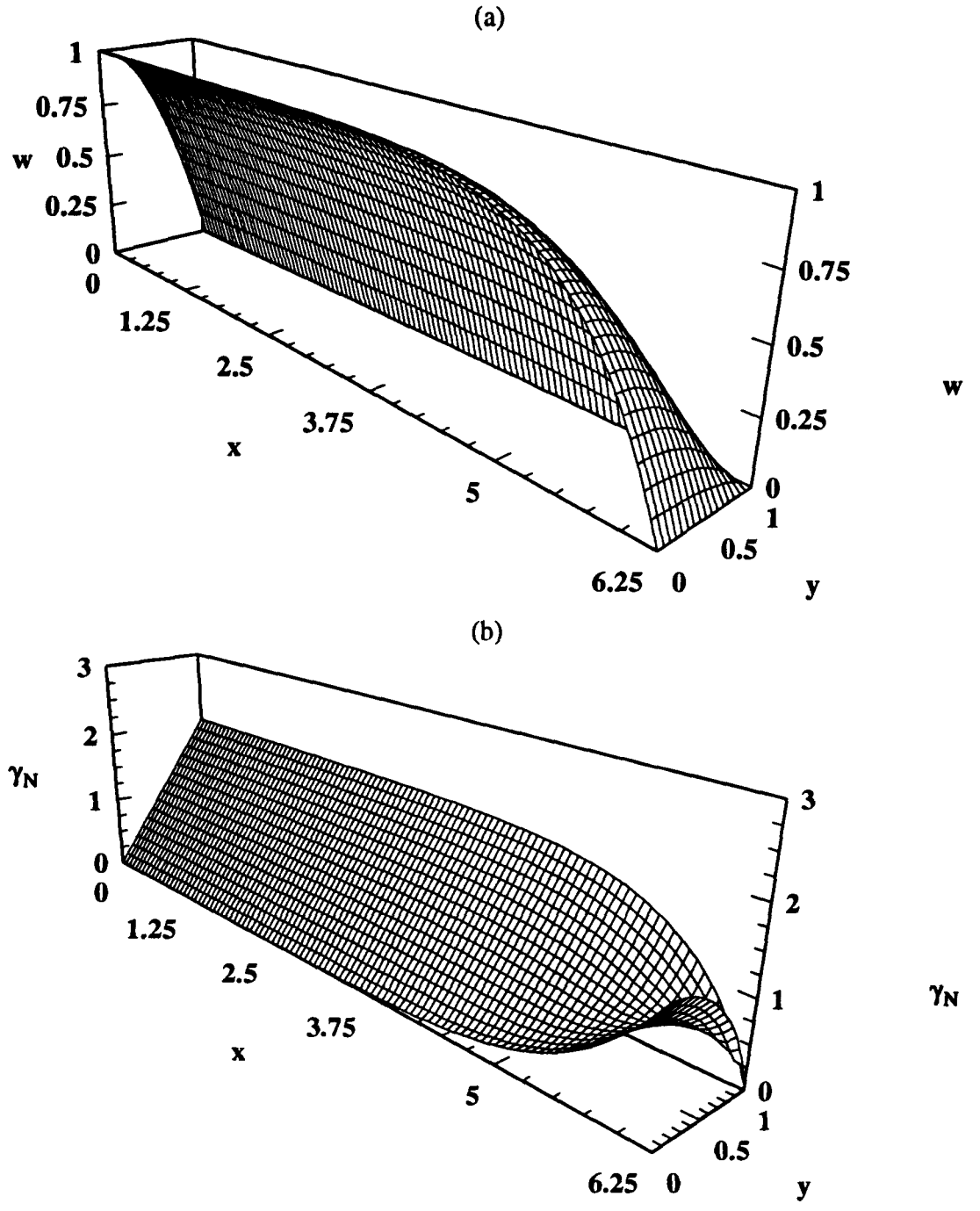

Figure 1. Longitudinal Newtonian velocity profile (a), and velocity gradient magnitude (b), in a rectangular duct with dimension ratio of 1:6.25.

resulting flow at the region of high concentration resembles a plug-like flow of an almost solid core moving in the surrounding suspension.

The above results, though reported for the first time, can be qualitatively anticipated from the basic characteristics of the shear-induced particle phenomena. The migration of particles due to shear rate and concentration gradients should result in particle accumulation at low shear regions which simultaneously, through the effective viscosity, affects the local shear and the velocity profile.

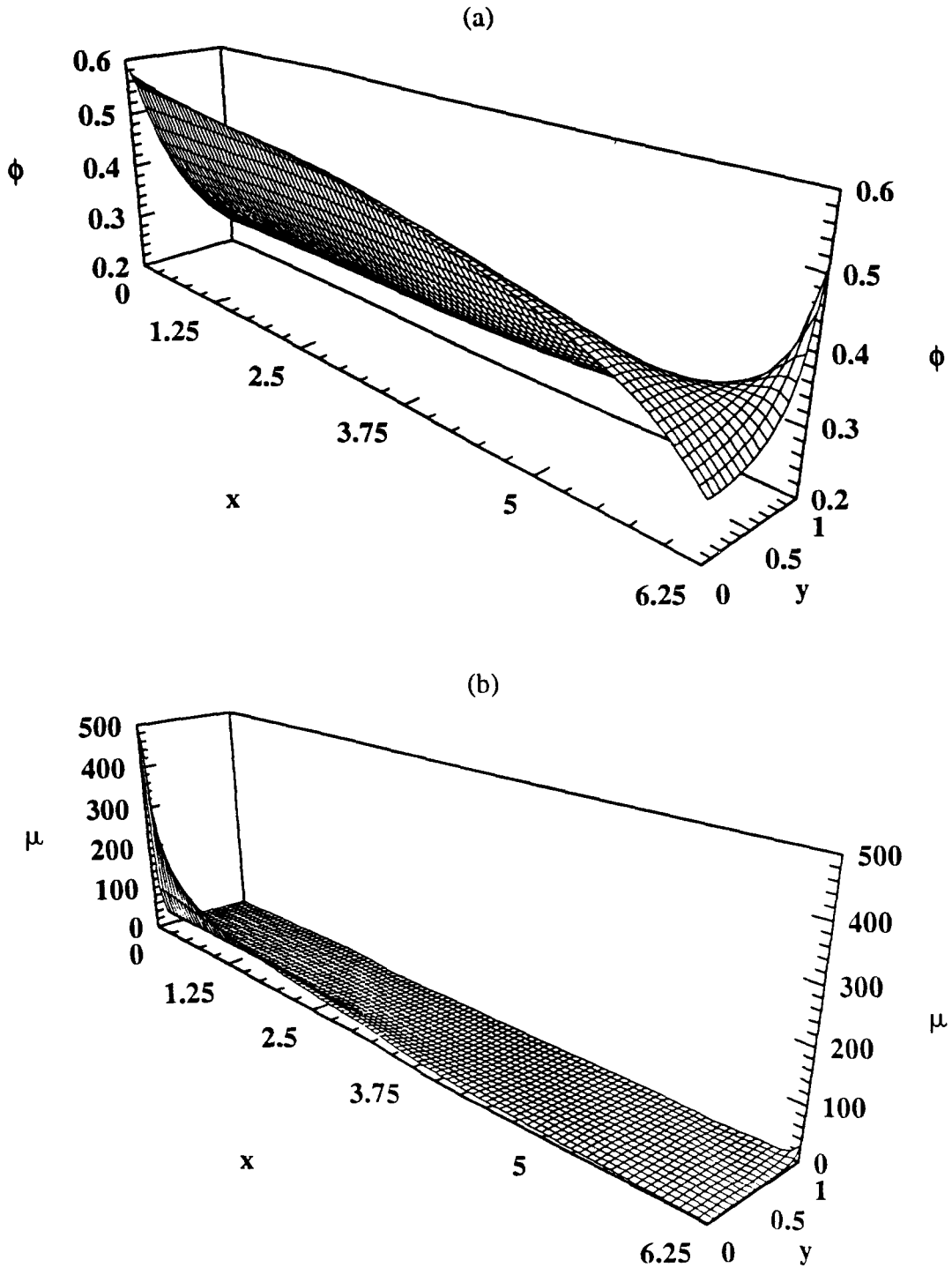

Figure 2. Concentration profile (a), and the distribution of effective viscosity (b), in a rectangular duct with dimension ratio of 1:6.25. Suspension concentration $\phi_s = 0.4$.

Yet a closer look at the results provides two interesting and not obvious phenomena. At the final stage, with

$$\frac{D\phi}{Dt} = 0,$$

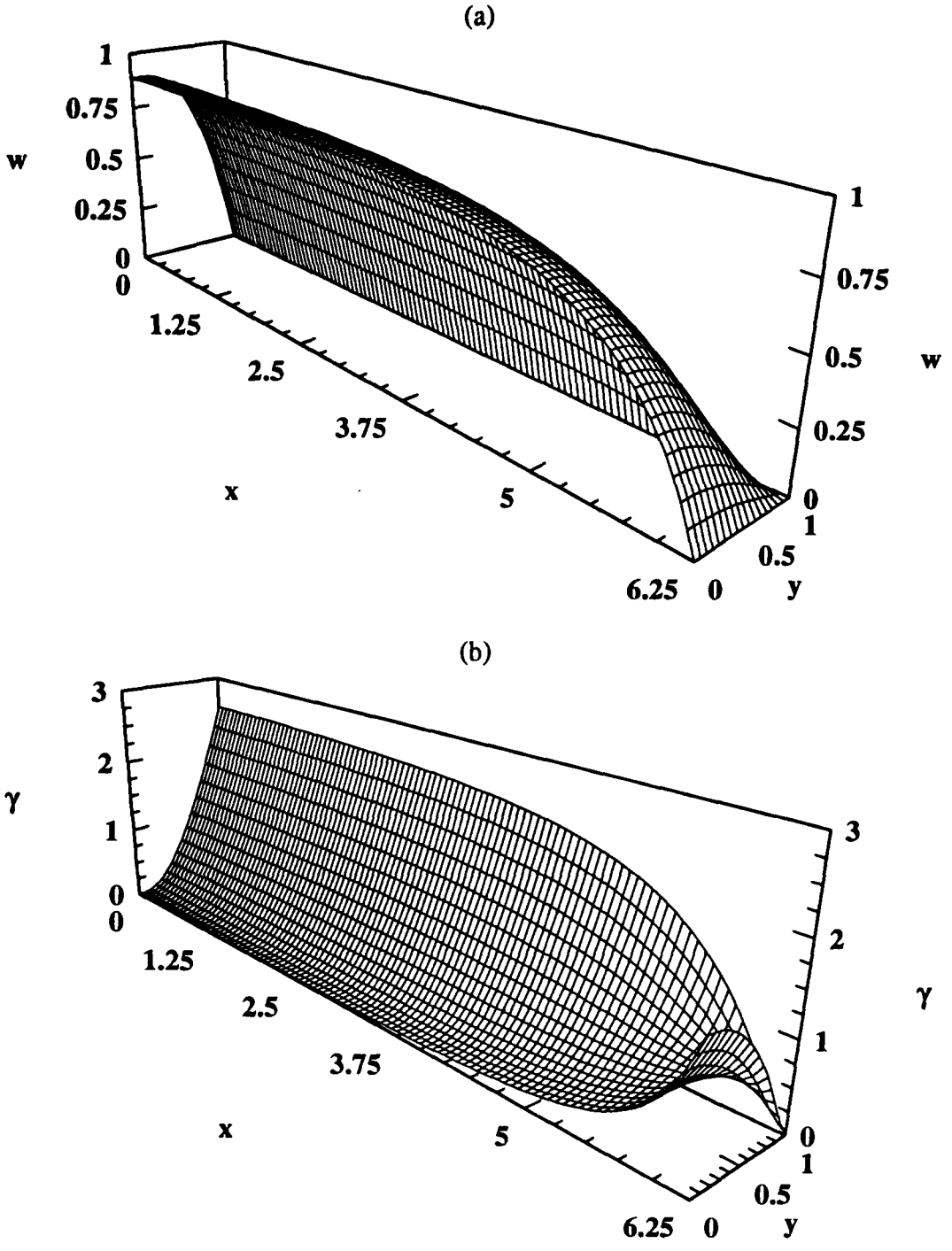

Figure 3. Final longitudinal velocity profile (a), and velocity gradient magnitude (b), in a rectangular duct with dimension ratio of 1:6.25. Suspension concentration $\phi_s = 0.4$.

the solution of [4] is $P = P_f$, a constant. Figure 5(a) shows the value of for various suspensions concentration. Similarly we examined the final value of the pressure gradient required to drive the flow $(dp/dz)_f$, relative to the initial Newtonian value $(dp/dz)_N$. At equal mass or volume flow rates this is equivalent to comparing the change in viscous dissipation of energy in the flowing suspension. In all cases considered, as shown in figure 5(b), dp/dz reduced considerably from the initial to the final flow state. This phenomena was already pointed out by Seifu *et al.*

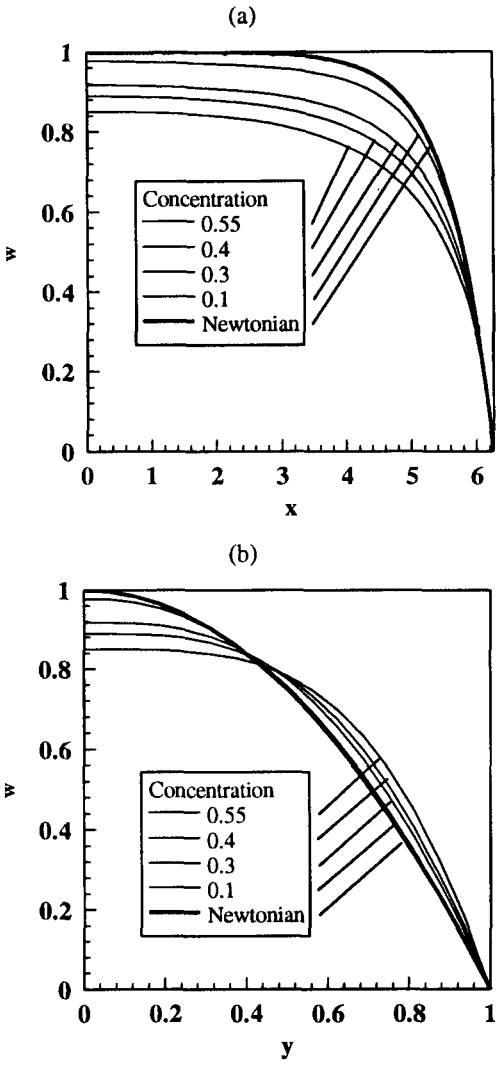

Figure 4. Longitudinal velocity profiles at final state of various suspensions flowing in a rectangular duct with dimension ratio of 1:6.25. (a) cross section along the wide axis, x, (b) cross section along the narrow axis, y.

(1994) for various other flows of concentrated suspensions exhibiting shear-induced particle migration.

Transient state. At any position along the duct (z coordinate) the suspension is in transient state, i.e. the velocity and concentration distributions in the cross section have not yet attained their final state profiles. It is sufficient to state here that the development of these profiles from a uniform concentration and a Newtonian velocity (figure 2) to those depicted by figures 3 and 4, is gradual and monotonous. The change in the pressure gradient along the flow is, however, more dramatic since a considerable portion of the drop in energy dissipation occurs already in the initial stages of the profiles development. This is shown clearly in figure 6 particularly for the relatively high concentrations. Small changes in particle concentrations and effective viscosity distributions induce considerable drop in power required to drive the flow. This, however, should not be interpreted as a possible method to reduce drag since, as is well known, any addition of a dispersed phase to a viscous fluid results in a positive change of the viscous dissipation.

Of particular interest are shear induced migration velocities of particles toward the low shear zone at the duct center at various dimensionless distances. These velocities along the long and short center axes are shown in figure 7 for the case $\phi_s = 0.4$. There is a significant difference between these fluxes. Along the short, y axis, we notice from figure 1(b) that, initially γ is almost linear.

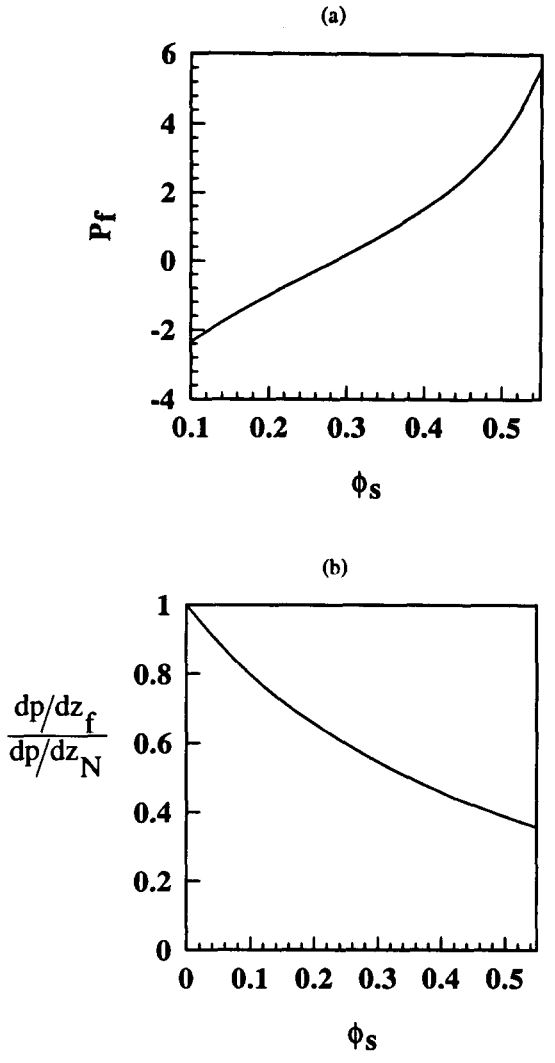

Figure 5. Final value of particle migration potential, P (a), and ratio between pressure drop at the entrance and pressure drop in final state of flow (b), along a rectangular duct with dimension ratio of 1:6.25 for various suspension concentrations.

Thus, with the initial unchanged uniform concentration, the particle flux at $z = 10^{-6}$ is driven by a constant shear gradient and is therefore uniform except where it is zero (near the wall where there is no penetration and at the center due to symmetry, see figure 7(b)). At larger distances, e.g. $z = 0.01$, concentration gradients developed and they oppose the shear rate gradients. This results in a clear maximum of the now rounded particle migration velocity profile at some intermediate location along the y axis.

Similar maxima are visible in the migration velocity profiles along the x axis (figure 7(a)). Here they are evident from the initial state and stem from the non-uniform profile of γ along this axis and the interaction with the wall. The migration profile shapes remain similar while their intensity reduces along the duct distance. Such behavior was obtained for all ϕ_s considered and was also obtained experimentally (see figure 10). However, the intensity of the maxima of migration velocities does not increase monotonically with ϕ_s as is shown in figure 8. At the entrance to the duct the migration velocity is maximal at the highest concentration. However, as flow develops it is clear that at a downstream position along the duct, maximal migration velocities are realized for some intermediate ϕ_s. Again, similar behavior was obtained experimentally (see figure 13(b)). This is a testimony for the competition between the different developments of the diffusion

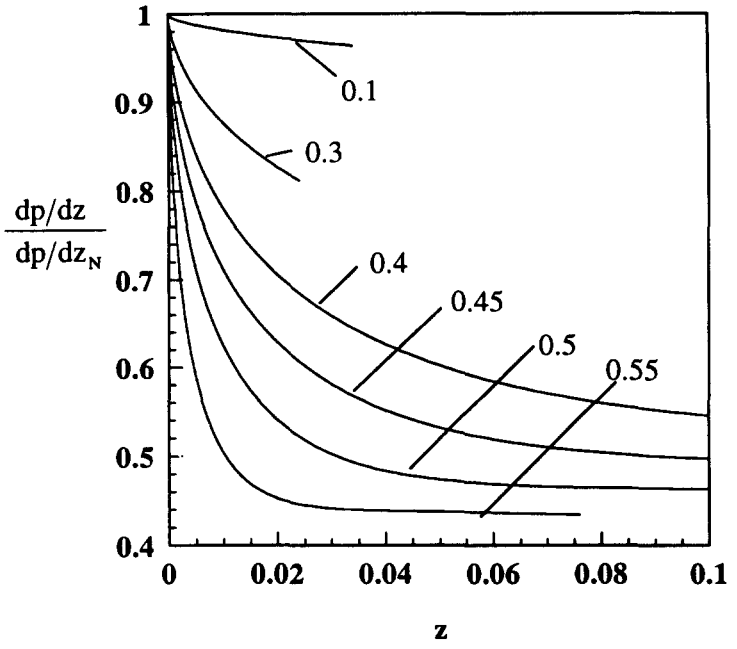

Figure 6. Pressure drop decline in a flow along a rectangular duct with dimension ratio of 1:6.25 for various suspension concentrations.

coefficient and the migration driving force in [3], D and ∇P respectively, in each case. Further discussion of this point is given in section 4 in view of the experimental findings.

3. EXPERIMENTAL RESULTS AND DISCUSSION

A detailed description of the experimental system is given in Part I. It consists of the flow apparatus, the suspension and the optical and electronic setups.

3.1. Flow system

The dimensions of the duct were chosen to ensure the existence of a slow viscous flow of the suspension and to create two regions of shear rate along the longitudinal velocity profile: a high shear rate close to the wall and a relatively flat profile at the cell center. The wide and narrow sides of the rectangle (in the x and y directions, respectively) were considerably large compared to the average particle diameter, 50 mm, 8 mm and 85 μm, respectively. Thus the three and two orders of magnitude ratios ensured that the suspension could be viewed as an effective continuum and that wall effects on individual particles were relevant only in small portions of the velocity profiles in the vicinity of the walls.

The continuous mixing of inlet flow ensured uniform flow and temperature distributions at the entrance to the channel. This uniform temperature is important to maintain a uniform effective viscosity and is most important to maintain the desired optimal refractive index difference.

3.2. Results and Discussion

Figure 9 shows vertical velocity profiles measured along the x axis, of flowing suspensions with various particle volume fractions, varying from $\phi_s = 0.1$–0.5, for different maximum center velocities. At each point 2000 measurements were collected and their average calculated. The profiles are very accurately reproducible. All profiles are normalized by the corresponding value of the center velocity. The clear symmetry of these profiles is a direct consequence of the careful introduction and mixing of the suspension at the inlet vessel and of the maintenance of the uniform temperature.

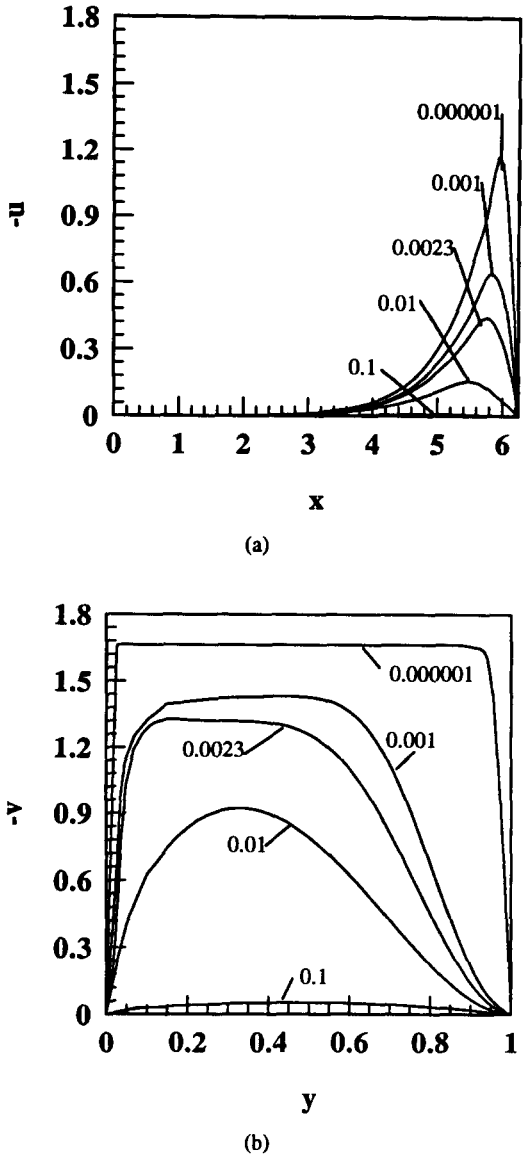

Figure 7. Lateral velocity profiles at different locations along a rectangular duct with dimension ratio of 1:6.25. (a) cross section along the wide axis, x, (b) cross section along the narrow axis, y. Suspension concentration $\phi_s = 0.4$.

The similarity of profiles of the same particle concentration at different center velocities is evident. Each of these figures contains also the calculated profile corresponding to the flow of a homogeneous viscous Newtonian fluid. At low particle volume fraction, as in figure 9(a) and (b) corresponding to $\phi_s = 0.1$ and 0.3, respectively, the measured profiles are identical with the Newtonian profile. This indicates that at the measurement location these suspensions behave as effective Newtonian fluids and that any deviation from homogeneity is negligible. For $\phi_s = 0.4$ (figure 9(c)) deviations of the normalized profiles from the Newtonian profile are noticeable. Although similar to each other for all maximum velocities they do not conform to the calculated profile. This difference becomes more pronounced at $\phi_s = 0.45$ (figure 9(d)). At $\phi_s = 0.5$ (figure 9(e)) where the normalized plots deviate from each other as well, indicating that, at these particle concentrations, even small deviations from homogeneity affect strongly the characteristics of the flowing suspension.

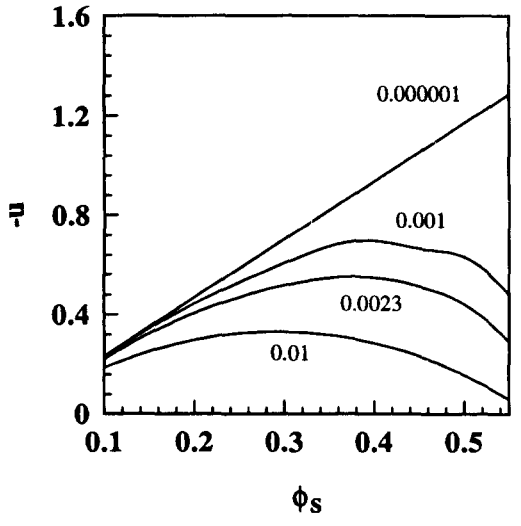

(a)

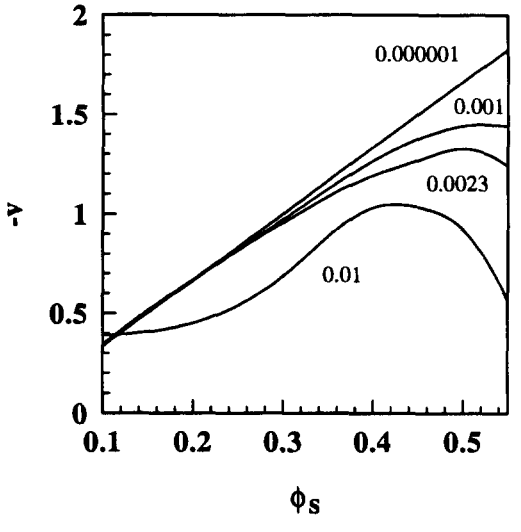

(b)

Figure 8. Maximal lateral velocity vs suspension concentration at different locations along a rectangular duct with dimension ratio of 1:6.25. (a) cross section along the wide axis, x, (b) cross section along the narrow axis y.

The key to understanding this behavior lies in the results obtained for the horizontal velocities (in the x direction) when measured at the same location points. The results of these measurements for the five particle volume fractions and for the various maximum velocities are assembled in figure 10. In all figures the symmetry is again evident, and zero velocities exist at the walls and at the center points. At all other points non-zero horizontal velocities were detected aiming toward the center. At $\phi_s = 0.1$ (figure 10(a)) the magnitude of this velocity is insignificant and falls within the range of reproducibility of the measured results ($< 15\ \mu$m/s). However, for all other concentrations the horizontal velocity is not negligible and velocimeter detects non negligible horizontal velocity components. These components are not an indication to a development of the macroscopic vertical velocity profile. Since these profiles are always fully developed as is predicted by viscous flow consideration and is confirmed by the measurements of the vertical and horizontal velocities at low particle concentration, $\phi_s = 0.1$. Thus, at higher particle concentration the horizontal profiles clearly indicate net drift induced by the presence of the particles. These profiles

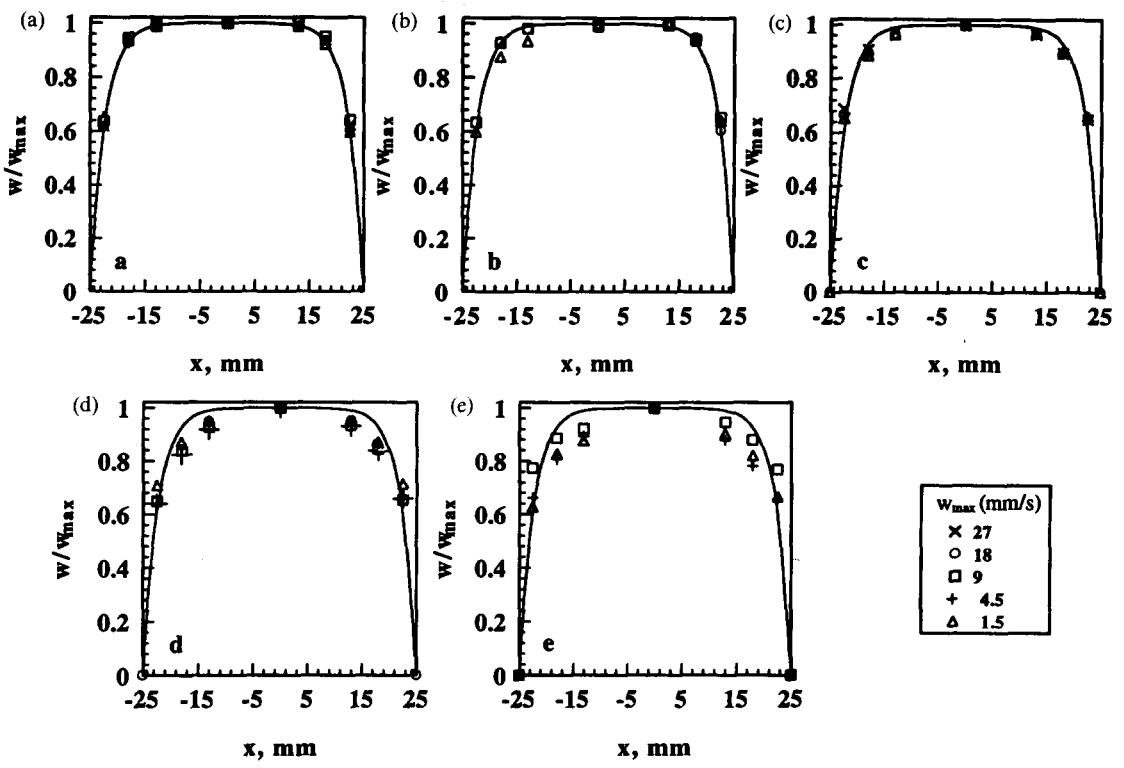

Figure 9. Measured suspension longitudinal velocities, normalized by the maximum center velocity, for various suspension concentration and flow rates. (a) $\phi_s = 0.1$; (b) $\phi_s = 0.3$; (c) $\phi_s = 0.4$; (d) $\phi_s = 0.45$; (e) $\phi_s = 0.5$.

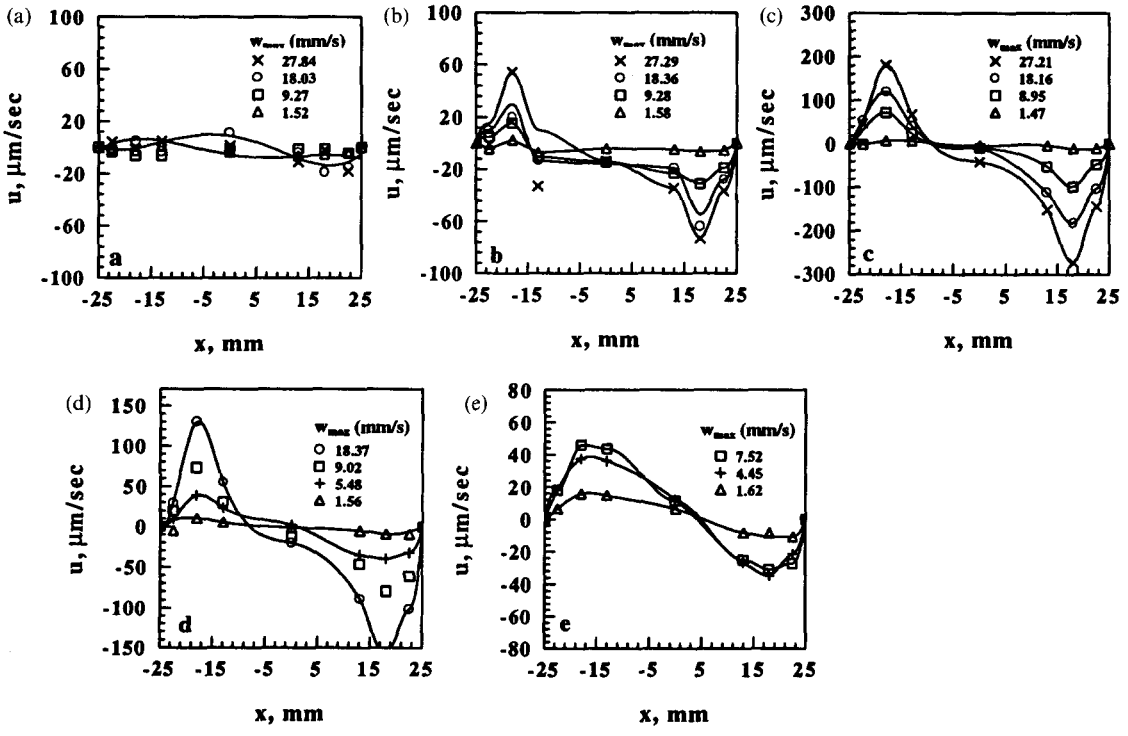

Figure 10. Horizontal velocity profiles for various suspension concentrations and flow rates. (a) $\phi_s = 0.1$; (b) $\phi_s = 0.3$; (c) $\phi_s = 0.4$; (d) $\phi_s = 0.45$; (e) $\phi_s = 0.5$.

are similar in shape to the corresponding horizontal particle velocities calculated by the phenomenological model and reported in figure 7(a).

The standard deviations of the measurements of the vertical and horizontal velocities were discussed in length in Part I. We bring here a summary of all STDs as is depicted in figure 11. The points indicate averages of the STDs of the three central points in each measured velocity profile. The shear intensity dependence common to all particle concentrations is evident from the linear dependence of the results on the maximum center velocity. However, for both vertical and horizontal measurements, the slopes are equal for all particle concentrations since the latter do not affect the shear intensity. The intersections of the lines with the ordinate reflect the part of the measurement not associated with the flow. In all cases, vertical and horizontal, the noise magnitude is less than 100 μm/s and under the assumption of flow independence can be subtracted from the total variance of the measurement.

When viewing the horizontal drift profiles of various suspensions at similar maximum vertical velocity (see figures 12(a)–(b)) it becomes clear that the dependence of the drift on suspension concentration is not trivial. All profiles obtain a maximum in the drift intensity near the wall. It is clear that the intensity of the measured horizontal velocity increases with particle concentration up to some maximum and then decreases as particle concentration becomes significantly high. In figure 13(a) we have plotted the change of the horizontal velocity, as measured 7 mm from the side walls, as a function of the maximum center velocity for each particle concentration. As is expected the drift increases monotonically with the increase of the shear rate intensity at the same location. The dependence appears linear and the rates of change, indicated by the lines slopes depend on the suspension concentration. The change of the maximum value of the measured drift with particle concentration is, however, not monotonic as was already suggested in figure 12. Figure 13(b) shows this change. At relatively low particle concentrations the dominant migration driving force is the gradient of shear intensity and the local changes of concentration at $z = 295$ mm are insignificant. This is also corroborated by the almost perfect Newtonian vertical velocity profiles for the low concentration (figure 9). Increase of particle concentration results in an increase of drift velocities and flux. At very high concentrations, however, the effective viscosity is increased considerably and the resistance to particle motion is greatly augmented. Furthermore, at these high concentrations any change in local concentration results in gradients in effective viscosity which oppose the

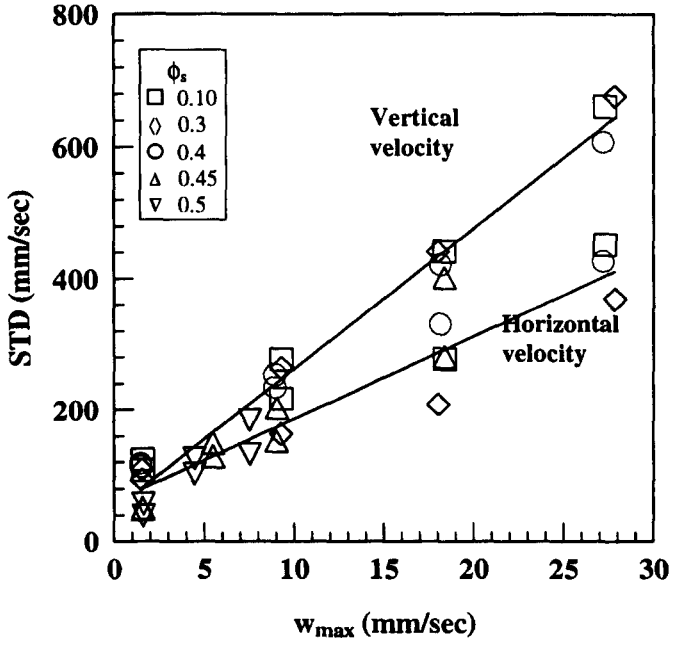

Figure 11. Standard deviation of vertical and horizontal velocity measurements at duct center region for various suspension concentrations and flow rates.

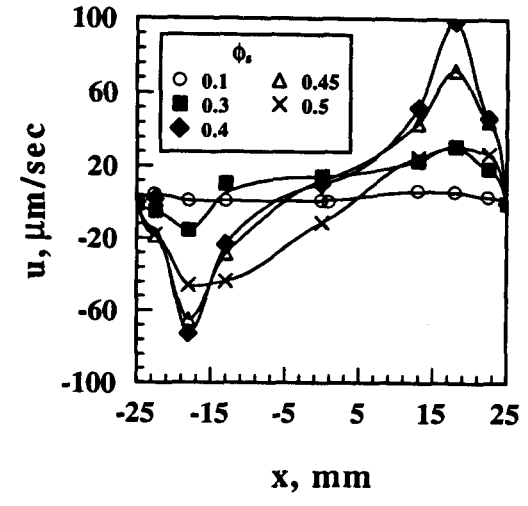

(a)

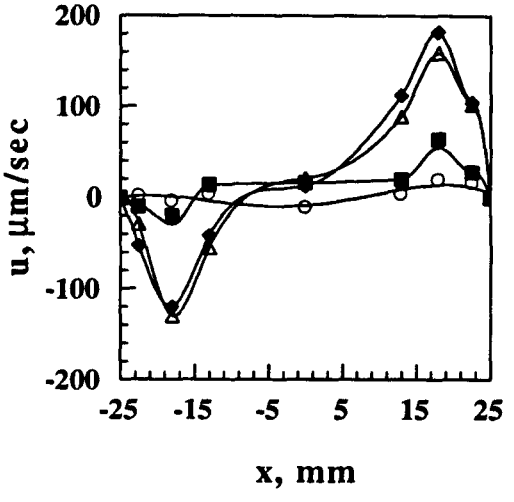

(b)

Figure 12. Horizontal drift profiles of suspensions with various concentrations. (a) $w_{max} = 9$ mm/s; (b) $w_{max} = 18$ mm/s.

migration and thereby adversely influence the net flux. Thus, the maxima appearing in the curves of figure 13(b). These observations agree with those predicted by the phenomenological model calculations (figure 8) where the maximum particle drift velocity was found for suspension concentration of approximately $\phi_s = 0.4$. Similar maximum in sedimenting concentrated suspensions, where self-diffusivities experienced a strong decrease for $\phi_s > 0.3$, were reported recently (Guazzelli 1995).

A comparison between the calculated predictions and the measured observations shows a qualitative similarity concerning velocity profiles and particle drift behavior. However, the quantitative agreement was found rather poor. The measurement point at $z = 295$ mm corresponds to a dimensionless distance of 0.0023. At this measurement point the theoretical calculations predict a migration velocity which is over an order of magnitude lower than the drift velocity detected by the laser–Doppler velocimeter. It should be noted that the drift velocity depends on the square of the size of the migrating particle. A possible explanation for this discrepancy may come from the tendency of particles to aggregate in the sheared suspension and migrate as clusters rather than as monodispersed individual particles. These clusters have a larger effective dimension thus increasing considerably the drift velocity. The formation of clusters has also been suggested by the

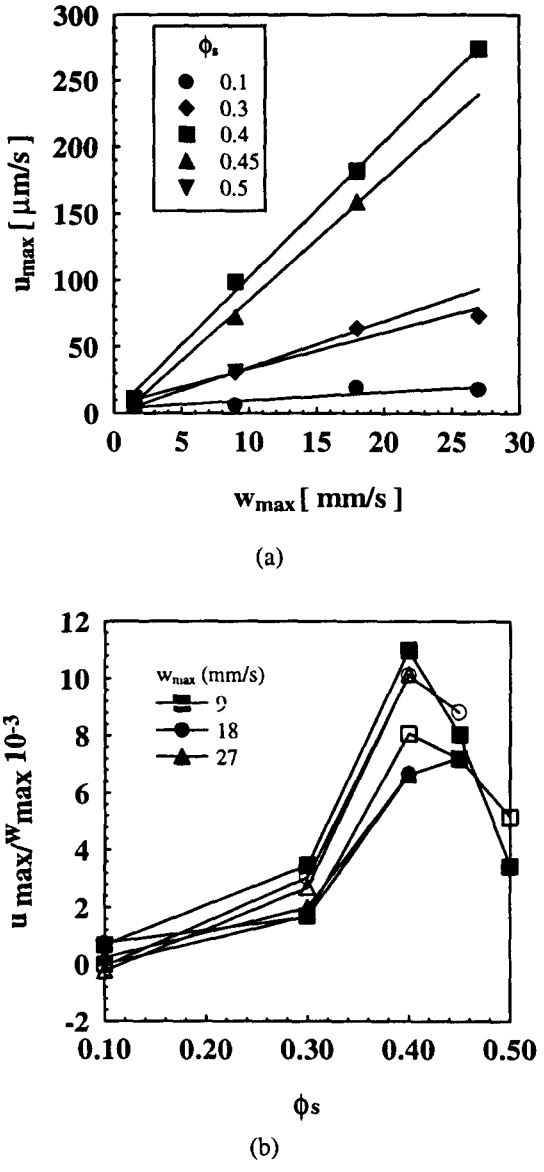

Figure 13. Maximum drift velocity for various suspension concentration and flow rate. (a) Linear dependence on flow rate; (b) dependence on concentration normalized by maximum vertical velocity for each run. Full and empty symbols indicate right and left sides of the measured profiles, respectively.

Stokesian dynamics simulations of bimodal suspensions of hydrodynamically interacting spheres (Chang and Powell 1993).

4. CONCLUSIONS

The improved application of the laser Doppler velocimetry technique in concentrated suspensions facilitated, for the first time, a direct measurement of particle migration velocities. For high concentrations, $\phi_s > 0.4$, a direct connection between particle lateral migration and changes in suspension velocity profiles is evident. The longitudinal profiles lose their Newtonian shape.

The measured lateral and longitudinal velocity profiles agree qualitatively with the model calculations based on the phenomenological models of Leighton and Acrivos (1987a) and Phillips *et al.* (1992), presented in this work.

The possibility of formulating a particle migration potential suggests that the particle flux may be driven by a single integral property of the suspension, a function of the local particle

concentration and suspension shear rate. The net flux diminishes when variations in the property vanish.

Acknowledgements—This research was supported by the Basic Research Foundation administered by the Israel Academy of Sciences and in part by Grant 92-00071 of the US–Israel Binational Science Foundation (BSF), Jerusalem, Israel. A Averbakh acknowledges support in part by the Israeli Ministry of Absorption.

REFERENCES

Averbakh, A., Shauly, A., Nir, A. and Semiat, R. (1997) Slow viscous flows of highly concentrated suspensions—part I: laser–Doppler velocimetry in rectangular ducts. *Int. J. Multiphase Flow* **23,** 409–424.

Chang, C. and Powell, R. L. (1993) Dynamic simulation of bimodal suspensions of hydrodynamically interacting spherical particles. *J. Fluid. Mech.* **253,** 1–25.

Eckstein, E. C., Bailey, D. G. and Shapiro, A. H. (1977) Self-diffusion of particles in shear flow of a suspension. *J. Fluid Mech.* **79,** 191–208.

Gadala-Maria, F. and Acrivos, A. (1980) Shear induced structure in a concentrated suspension of solid spheres. *J. Rheol.* **24,** 799–814.

Guazzelli, E. (1995) Experiments on sedimentation: particle velocity fluctuations and hydrodynamic self-diffusion of sedimenting non-Brownian spheres. *IUTAM Symposium on Hydrodynamic Diffusion of Suspended Particles*. Estes Park Co.

Karnis, A., Goldsmith, H. L. and Mason, S. G. (1996) The kinetics of flowing dispersions—I. Concentrated suspensions of rigid particles. *J. Colloid Sci.* **22,** 531–553.

Koh, C. J., Hookham, P. and Leal, L. G. (1994) An experimental investigation of concentrated suspension flows in a rectangular channel. *J. Fluid Mech.* **266,** 1–32.

Kriger, I. M. (1972) Rheology of monodisperse lattices. *Adv. Colloid Interface Sci.* **3,** 111–136.

Leighton, D. (1985) The shear induced migration of particulates in concentrated suspensions. Ph.D. thesis, Stanford Univ., Stanford, CA.

Leighton, D. and Acrivos, A. (1986) Viscous resuspension. *Chem. Eng. Sci.* **41,** 1377–1384.

Leighton, D. and Acrivos, A. (1987a) The shear-induced migration of particles in concentrated suspensions. *J. Fluid Mech.* **181,** 415–439.

Leighton, D. and Acrivos, A. (1987b) Measurement of shear-induced self-diffusion in concentrated suspensions of spheres. *J. Fluid Mech.* **177,** 109–131.

Phillips, R. J., Armstrong, R. C., Brown, R. A., Graham, A. L. and Abbott, J. R. (1992) A constitutive equation for concentrated suspensions that accounts for shear-induced particle migration. *Phys. Fluids A* **4,** 30–40.

Press, W. H., Teukolsky, S. A., Vetleriling, W. T. and Flannery, B. P. (1992) *Numerical Recipes in Fortran, The Art of Scientific Computing*, 2nd Edition. Cambridge University Press, Cambridge.

Schaflinger, U., Acrivos, A. and Zhang, K. (1990) Viscous resuspension of sediment within a laminar and stratified flow. *Int. J. Multiphase Flow* **16,** 567–578.

Schlichting, H. (1965) *Boundary Layer Theory*, 6th Edition. McGraw-Hill, New York.

Seifu, B., Nir, A. and Semiat, R. (1994) Viscous dissipation rate in concentrated suspensions. *Phys. Fluids* **6,** 3191–3289.